Inorganic Chemistry

Article

pubs.acs.org/IC

Characterization of Water Coordination to Ferrous Nitrosyl Complexes with *fac*-N_2O, *cis*-N_2O_2, and N_2O_3 Donor Ligands

John McCracken,*[,†] Patrick J. Cappillino,[‡,§] Joshua S. McNally,[‡] Matthew D. Krzyaniak,[†] Michael Howart,[†] Paul C. Tarves,[‡] and John P. Caradonna*[,‡]

[†]Department of Chemistry, Michigan State University, East Lansing, Michigan 48824, United States

[‡]Department of Chemistry, Boston University, Boston, Massachusetts 02215, United States

[§]Department of Chemistry and Biochemistry, University of Massachusetts at Dartmouth, North Dartmouth, Massachusetts 02347, United States

Supporting Information

ABSTRACT: Electron paramagnetic resonance (EPR) experiments were done on a series of $S = {}^3/_2$ ferrous nitrosyl model complexes prepared with chelating ligands that mimic the 2-His-1-carboxylate facial triad iron binding motif of the mononuclear nonheme iron oxidases. These complexes formed a comparative family, $\{FeNO\}^7(N_2O_x)(H_2O)_{3-x}$ with $x = 1-3$, where the labile coordination sites for the binding of NO and solvent water were fac for $x = 1$ and cis for $x = 2$. The continuous-wave EPR spectra of these three complexes were typical of high-spin $S = {}^3/_2$ transition-metal ions with resonances near $g = 4$ and 2. Orientation-selective hyperfine sublevel correlation (HYSCORE) spectra revealed cross peaks arising from the protons of coordinated water in a clean spectral window from $g = 3.0$ to 2.3. These cross peaks were absent for the $\{FeNO\}^7(N_2O_3)$ complex. HYSCORE spectra were analyzed using a straightforward model for defining the spin Hamiltonian parameters of bound water and showed that, for the $\{FeNO\}^7(N_2O_2)(H_2O)$ complex, a single water conformer with an isotropic hyperfine coupling, $A_{iso} = 0.0 \pm 0.3$ MHz, and a dipolar coupling of $T = 4.8 \pm 0.2$ MHz could account for the data. For the $\{FeNO\}^7(N_2O)(H_2O)_2$ complex, the HYSCORE cross peaks assigned to coordinated water showed more frequency dispersion and were analyzed with discrete orientations and hyperfine couplings for the two water molecules that accounted for the observed orientation-selective contour shapes. The use of three-pulse electron spin echo envelope modulation (ESEEM) data to quantify the number of water ligands coordinated to the $\{FeNO\}^7$ centers was explored. For this aspect of the study, HYSCORE spectra were important for defining a spectral window where empirical integration of ESEEM spectra would be the most accurate.

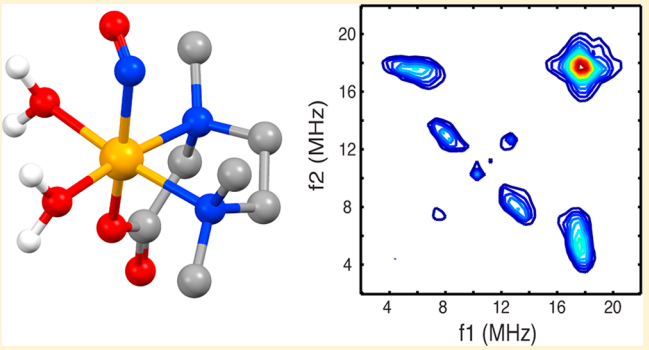

INTRODUCTION

The mononuclear nonheme iron oxygenases (MNOs) catalyze a broad range of biologically important reactions using a highly conserved iron binding site that is often referred to as the 2-His-1-carboxylate "facial triad".[1,2] For this structural motif, the metal ion is bound to the enzyme by the facial coordination of the imidazole side chains of two histidines and the carboxylate side chain of either glutamate or aspartate residues. This NNO coordination scheme leaves three open coordination sites that are fac to one another to accommodate possible binding of the substrate, cofactor, and molecular oxygen during catalysis. Outside of this common iron-binding scheme, the enzymes that belong to this family show very little sequence homology.[3] As a result, details of the chemistry that occurs at the open coordination positions on iron and the structure of the surrounding protein environment are central to understanding the catalytic mechanism.

Our specific interest in MNOs is in the oxygen-activating pterin-dependent hydroxlase, phenylalanine hydroxylase (PheH), which catalyzes hydroxylation of the phenyl side chain of the substrate L-phenylalanine (L-phe) to form L-tyrosine.[4,5] This is an important first step in the metabolism of phe, with dysfunction in the enzyme leading to the disease Phenylketonuria (PKU).[6] Catalytic turnover requires binding of the substrate L-phe, a cofactor, tetrahydrobiopterin (BH_4), and molecular oxygen. The foundation for understanding structure–function relationships and the catalytic mechanism of PheH comes from a series of X-ray crystallographic structures of a truncated form of the enzyme with the iron in its active oxidation state, Fe^{II}. Structures of the enzyme crystallized without L-phe and BH_4, cocrystallized with BH_4, and cocrystallized with BH_4 and soaked with "slow" substrates,

Received: April 8, 2015
Published: June 19, 2015

DOI: 10.1021/acs.inorgchem.5b00788
Inorg. Chem. 2015, 54, 6486–6497

thienylalanine and norleucine, are available.[7−9] Overall, these structures show that neither cofactor BH_4 nor the "slow" substrates bind directly to the Fe^{II} center. However, they do bind to the active site as second-sphere ligands, and their coordination leads to conformational changes in the protein that prepare the system for oxygen binding and catalysis. The structural information for this enzyme is incomplete. The enzyme has not been crystallized with substrate, and attempts to soak L-phe in crystals grown with truncated enzyme and BH_4 resulted in dissolution of the crystals.[8] In addition, PheH is allosterically regulated by substrate L-phe, and the truncated form of the protein that has been crystallized lacks the regulatory domain.[10−13]

Important information regarding structure−function relationships has also come from spectroscopic measurements. Specifically, X-ray absorption spectroscopy and variable-temperature variable-field magnetic circular dichroism spectroscopy have provided information on the changes in Fe^{II} coordination that accompany the substrate and cofactor binding and that facilitate its reactivity with molecular oxygen.[11−13] Rapid freeze quench Mössbauer spectroscopy has been used to identify a key iron(IV) oxo intermediate in tyrosine hydroxylase, another enzyme in this family.[14] While these spectroscopic methods have the advantage of being able to use a full-length enzyme and biologically relevant substrates and cofactors, they probe the electronic structure of iron and provide details regarding its coordination geometry and oxidation−reduction state.

In an effort to structurally characterize Fe^{II} ligation and binding of the substrate and cofactor to the catalytic site of MNOs, we have employed the pulsed electron paramagnetic resonance (EPR) method of electron spin echo envelope modulation (ESEEM).[15] Our studies make use of the methodology first employed by Rich et al.[16] and developed fully by the Lipscomb[17−19] and Hoffman[20−22] laboratories for the study of MNOs. Specifically, we used NO as a surrogate for molecular oxygen to poise the $S = 2$ Fe^{II} center in an $S = {}^3/_2$ $\{FeNO\}^7$ form that is amenable to X-band EPR spectroscopy.[23] In addition to creating an EPR-active catalytic site, NO coordination serves to approximate oxygen binding and the Fe−NO bond provides a reference for the interpretation of ligand hyperfine couplings in terms of structure.[24,25]

An important question for understanding the catalytic mechanism of PheH and structural changes at the Fe^{II} site associated with allosteric control of the catalytic activity involves the measurement and quantification of bound water. Because ligand hyperfine interactions for water molecules bound to paramagnetic transition ions are typically characterized by large anisotropic proton couplings,[26] their contributions to ESEEM spectra should be easily distinguished from proton couplings arising from the histidine ligands using the two-dimensional, four-pulse hyperfine sublevel correlation (HYSCORE) technique.[27,28] Indeed, previous HYSCORE studies of high-spin met-myoglobin yielded highly resolved ^{14}N and ^1H cross peaks from heme, histidylimidazole, and coordinated water.[29,30] Unfortunately, preliminary HYSCORE studies of $\{FeNO\}^7$ adducts of PheH proved too complex to definitively assign cross peaks to water molecules coordinated to the $S = {}^3/_2$ center.[31] As a result of this early setback, we turned to a series of iron(II) model complexes, **1**−**3** respectively containing the ligands 2-[[[2-(dimethylamino)-ethyl]methyl]amino]acetic acid (N_2O_1), 2,2′-[ethane-1,2-diylbis(methylazanediyl)]diacetic acid (N_2O_2), and 2,2′-[2-[[(carboxymethyl)methyl]amino]ethylazanediyl]diacetic acid (N_2O_3) (Scheme 1). As demonstrated by X-ray crystallographic characterization, each of these ligands presents a core facial N,N,O binding motif to iron(II), but they differ in the number of carboxylate ligands so that complexes with one (N_2O_3), two (N_2O_2), and three (N_2O) open-coordination sites are realized.[32] Treatment with NO in aqueous buffer yielded three complexes, $\{FeNO\}^7(N_2O)(H_2O)_2$ (**1·NO**), $\{FeNO\}^7(N_2O_2)(H_2O)$ (**2·NO**), and $\{FeNO\}^7(N_2O_3)$ (**3·NO**), that were studied with continuous-wave (cw) EPR, ESEEM, and HYSCORE at the X band. Our results provide a protocol for detecting, characterizing, and possibly quantifying water bound to the high-spin $S = {}^3/_2$ $\{FeNO\}^7$ adducts of MNOs.

Scheme 1. Structures of $1-FeN_2O_1$ (Left), $2-FeN_2O_2$ (Middle), and $3-FeN_2O_3$ (Right)

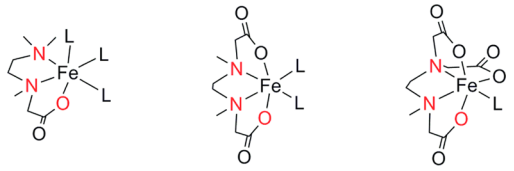

EXPERIMENTAL SECTION

Sample Preparation. Solvents used for sample preparation were freeze−pump−thawed for four cycles. All manipulations involving ferrous complexes and nitrosyl adducts were carried out in an inert-atmosphere (N_2) glovebox, except where noted. Nitric oxide (NO) gas (99+%) was purchased from Air Gas (Maumee, OH) and used without further purification. The ferrous complexes were prepared by literature procedures.[32] Stock solutions of **1**−**3** were prepared in Schlenk flasks using degassed H_2O- or D_2O-based and pH 6.5 3-(*N*-morpholino)propanesulfonic acid (MOPS) buffer. The flask was evacuated, and the headspace above the stirring sample was subsequently charged with 3−5 PSI of NO gas. The colorless solution turned immediately orange upon formation of the nitrosyl complex. The sample was allowed to stir for ∼1 min, the flask was evacuated, and the sample was brought back into the inert-atmosphere glovebox for further manipulation. Samples were then diluted to 5 mM with degassed 50:50 glycerol/$H(D)_2O$ as the glassing agent for a ∼40% final glycerol content. The samples were loaded into EPR tubes, frozen in $N_2(l)$, and shipped in a cryogenic shipping container charged with $N_2(l)$.

EPR Spectroscopy. cw-EPR and pulse EPR experiments were performed at X band with a Bruker E-680X spectrometer equipped with an ER4118X-MD-5-W1 probe that featured a 5 mm dielectric resonator. Sample temperatures were maintained at 4.0 K using an Oxford Instruments CF-935 liquid-helium cryostat and a model ITC-503 temperature controller. For cw-EPR measurements, the probe was critically coupled and a nonsaturating microwave power of 6.3 μW was used. Data were collected over a magnetic field range of 120−360 mT using a microwave frequency of 9.68 GHz, a magnetic field modulation amplitude of 0.8 mT, and a field modulation frequency of 10 kHz. All spectra were single scans and were collected with a time constant of 40 ms.

Pulse EPR data were collected under the same conditions with the sample probe overcoupled to the extent that a $\pi/2$ pulse of 16 ns (full-width at half maximum, fwhm) duration required a peak microwave power of 200 W. Three-pulse ESEEM data were collected using the standard $(\pi/2-\tau-\pi/2-t-\pi/2)$ sequence together with a four-step phase cycling scheme for eliminating contributions from two-pulse echoes and offset voltages.[33] Because the samples studied in this work showed T_2* values of approximately 100 ns, τ values were set to either the first or second integer multiple of the period of the ^1H Larmor

DOI: 10.1021/acs.inorgchem.5b00788
Inorg. Chem. 2015, 54, 6486−6497

frequency at each magnetic field position studied. The values for t were scanned from 40 ns to over 6 μs using a 12 ns time increment. Pulse sequence repetition rates of 1 kHz were used in our data acquisition, with each data point representing an average of 800 events. Three-pulse ESEEM spectra were derived from time domain data that were normalized by the division of a biexponential background decay function from the real portion of the data. The resulting modulation function was then processed by subtracting a second-order polynomial to remove the unmodulated component, tapered with a Hamming window, zero-filled to 1024 points, and Fourier-transformed. Absolute value spectra are presented.

HYSCORE data were collected using a four-pulse sequence ($\pi/2-\tau-\pi/2-t_1-\pi-t_2-\pi/2$). Most of the data were collected using a single microwave channel with $\pi/2$ pulses of 16 ns fwhm and π pulse widths of 28−32 ns. Data collected using a separately attenuated microwave channel to allow for both the $\pi/2$ and π pulse widths to be set to 16 ns fwhm (800 W peak power) showed diagonal peak amplitudes that were reduced by a factor of 2 but gave similar intensities for the cross peaks that were analyzed in this study.[28] τ values were set as described above, while t_1 and t_2 were scanned from 40 ns to just over 2 μs using a 16 ns time increment. Data sets of 128 × 128 time points were collected. A four-step phase cycling scheme was used to eliminate unwanted echoes from the data.[34] HYSCORE data were processed using a second-order polynomial to subtract the background decay in each time dimension, followed by application of a Hamming window, data set extension to 256 points, and two-dimensional fast Fourier transform. The absolute values of the resulting frequency spectra are presented as contour plots using a plotting threshold of 10−15% of the maximum peak amplitude.

Analysis. cw-EPR spectra were analyzed using the "pepper" module of *EasySpin* 4.5.5[35] running in the MATLAB 2014a environment (The Mathworks, Natick, MA). All three of the $\{FeNO\}^7(N_2O_x)(H_2O)_{3-x}$ samples showed nearly axial line shapes with features near $g = 4$ and 2. Such spectra are typical for $S = {}^3/_2$ paramagnetic centers, where the EPR spectrum originates from the $m_s = \pm{}^1/_2$ Kramers doublet as a result of a large, positive spin−orbit coupling interaction. The spin Hamiltonian used to model these data consisted of a zero-field-splitting (ZFS) term and an isotropic, spin-only, electronic Zeeman term (eq 1).[36] β_e and **B** in eq 1 are the Bohr magneton and applied magnetic field vector, respectively.

$$\hat{H} = D\left[\hat{S}_z^{\,2} - \frac{5}{4} + \frac{E}{D}(\hat{S}_x^{\,2} - \hat{S}_y^{\,2})\right] + g_0\beta_e\hat{\underset{\sim}{S}}\cdot\mathbf{B} \tag{1}$$

D represents the ZFS interaction and has been estimated from previous EPR, magnetic susceptibility, and Mössbauer studies of NO-treated nonheme Fe^{2+} enzymes and other $\{FeNO\}^7$ model complexes to be approximately 3.0×10^5 MHz ($10\ cm^{-1}$).[17,19,25,37] For our analyses, we set $D = 3.0 \times 10^5$ MHz and varied $|E|$ and the intrinsic EPR line widths, ΔH_x and ΔH_y, associated with the x and y canonical orientations of the ZFS interaction to fit the cw-EPR spectrum over an interval of 65 mT in the $g = 4$ region. The value of g_0 was adjusted to align the simulations with the data and was set to 2.015 for analysis of the spectra obtained in this study. The quality of our cw-EPR simulations was judged by determining a normalized χ^2 value (eq 2), where the sum is over N data points in the $g = 4$ region, y_i^{exp} and y_i^{calc} are the experimental and calculated spectral amplitudes at a given magnetic field position, and L is the number of adjustable parameters for the simulation. The standard deviation for these spectra, σ, was fixed at 2% of the maximum spectral amplitude for each data set. Parameters were varied to achieve a minimum in χ^2 using the function "fminsearch" that is resident in MATLAB.

$$\chi_n^{\,2} = \frac{\sum_{i=1}^{N}\frac{(y_i^{exp} - y_i^{calc})^2}{\sigma^2}}{N - L} \tag{2}$$

Proton HYSCORE spectra were analyzed using the "saffron" module of *EasySpin* 4.5.5.[38] These calculations were based on an $S = {}^3/_2$ electron-spin system and used the $|E|/D$ and g_0 values obtained from analysis of the cw-EPR spectra. Our task for these simulations was to model the HYSCORE response of water molecules bound to the $\{FeNO\}^7$ paramagnetic center. For each water proton, the spin Hamiltonian that describes its ligand hyperfine coupling is given by the sum of the nuclear Zeeman and electron−nuclear hyperfine coupling terms (eq 3).

$$\hat{H} = -\gamma_p\hat{\underset{\sim}{I}}\cdot\mathbf{B} + \hat{\underset{\sim}{S}}\cdot\mathbf{A}\cdot\hat{\underset{\sim}{I}} \tag{3}$$

$\hat{I}$ and $\hat{S}$ in eq 3 are the nuclear and electron-spin angular momentum operators, respectively, **B** is the applied magnetic field vector, and γ_p is the proton gyromagnetic ratio. **A** is the hyperfine coupling matrix that has been transformed into the principal axis system (PAS) of the ZFS interaction.

Previous single-crystal ENDOR studies of $Cu(H_2O)_6^{2+}$ showed that the proton hyperfine coupling of bound water molecules was primarily anisotropic in nature. For water ligands bound equatorially to Cu^{II}, the isotropic, or scalar, portion of the proton hyperfine interaction was found to be ≤1 MHz even though considerable unpaired spin density resides on the coordinated oxygen atom. The anisotropic portion of the proton hyperfine couplings was found to be of rhombic symmetry. For the axially bound water ligands of this complex, the authors measured an isotropic proton hyperfine coupling of zero and found that the anisotropic portion of the coupling was of axial symmetry and in line with values that could be predicted using the point dipole−dipole approximation.[26] Recent ENDOR studies of $\{FeNO\}^7$ adducts of the nonheme iron enzyme 1-aminocyclopropane-1-carboxylic acid oxidase have shown that the ligand hyperfine couplings for the coordinated histidine nitrogen atoms and the nitrogen atom of coordinated NO are in the 10 MHz range,[22] weaker than the corresponding couplings measured for histidyl nitrogen coordinated equatorially to Cu^{II} in proteins and model complexes.[39,40] These results provided a framework for modeling the proton hyperfine coupling tensors for water molecules bound to Fe^{II} in our model complexes. Specifically, the hyperfine interaction was modeled with a simple dipolar coupling tensor whose principal values were given by $(A_{iso} - T, A_{iso} - T, A_{iso} + 2T)$ with $A_{iso} = 0$, and with the principal axis of the tensor being directed along a line connecting Fe^{II} with the coupled proton.

$$T = \left(\frac{\mu_0}{4\pi}\right)\frac{g_0 g_n \beta_e \beta_n}{hr^3} \tag{4}$$

To be used in an ESEEM or HYSCORE simulation, the diagonal hyperfine tensor described above must be transformed into the PAS of the ZFS interaction. In *EasySpin*, this is done with a Euler transformation that uses a $zy'z'$ rotation scheme described by the Euler angles α, β, and γ, respectively. Because the hyperfine tensor has axial symmetry, only the β and γ angles need to be specified for each proton. In practice, specifying these angles was simplified because of the fixed geometric relationship between the two protons of a discrete water ligand, our knowledge of the molecular structure, and electronic structure calculations that place the principal axis of the ZFS interaction within 5° of the Fe−NO bond.[24] For our simulations, we adopted an elementary picture of the water molecule, with the oxygen atom being sp^3-hybridized and the ligand coordinating to Fe^{II} through one of the oxygen atoms' lone electron pairs. Using this model, the protons could be located on the base of a cone, approximately 120° apart, with a symmetry axis that coincided with the Fe−OH_2 bond. Then, assuming an Fe^{II}−O bond length of 2.0 Å, an O−H bond length of 1.0 Å, and an Fe−O−H bond angle of 110°, the Euler angles needed to specify the transformations for both of the water protons were determined from the angles that orient the Fe^{II}−OH_2 bond with respect to the ZFS axis system and a rotation angle that describes the orientation of the two protons about the bond axis. This approach to defining the hyperfine tensor transformation angles for the two protons of a bound water molecule is summarized in Scheme 2. It does not reduce the number of angles that need to be specified to transform the proton hyperfine tensors because one still must provide polar and azimuthal angles to position the Fe−O bond in the ZFS axis system, θ_{bond} and ϕ_{bond}, along with β_{rot} and $\Delta\beta$ to define the positions of the protons on the cone base (Scheme 2b). However,

DOI: 10.1021/acs.inorgchem.5b00788
Inorg. Chem. 2015, 54, 6486−6497

Scheme 2. Model Used To Determine the Euler Angles for Describing Coordinated Water Proton Hyperfine Couplings As Described in the Text[a]

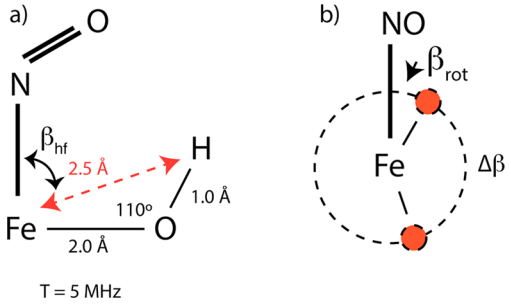

[a](a) Elementary structure used to develop eqs 5−8. T is the dipolar coupling calculated using eq 4 and an Fe−H distance of 2.5 Å. (b) View down the Fe−OH_2 bond showing the relationship between the Fe−NO bond axis and rotation angles that position the water protons.

this description makes it easier to visualize the transformations in terms of structure and to understand the limited range over which some of the angles need to be varied in simulations. The geometric relationships describing the transformations of the hyperfine tensors that need to be done for protons 1 and 2 of a bound water molecule having the geometry described above (Scheme 2) are given in eqs 5−8.

$$\beta_{hf1} = \theta_{bond} - \tan^{-1}[0.94\cos(\beta_{rot})/2.34] \quad (5)$$

$$\gamma_{hf1} = \phi_{bond} - \tan^{-1}[0.94\sin(\beta_{rot})/2.34] \quad (6)$$

$$\beta_{hf2} = \theta_{bond} - \tan^{-1}[0.94\cos(\beta_{rot} + \Delta\beta)/2.34] \quad (7)$$

$$\gamma_{hf2} = \phi_{bond} - \tan^{-1}[0.94\sin(\beta_{rot} + \Delta\beta)/2.34] \quad (8)$$

Because water ligands bound to Fe^{II} are expected to be cis to the Fe−NO bond axis, the value of θ_{bond} should be close to 90°. The near axial symmetry of the cw-EPR spectrum reduces the importance of ϕ_{bond}, but if two water molecules are considered in a simulation, the ϕ_{bond} values should be approximately 90° apart. Finally, the value of $\Delta\beta$ should fall in a range that is ±20° from our elementary starting value of 120°. In practice, the hyperfine couplings for the protons of a water ligand were specified in our simulations by providing discrete values for the dipolar couplings, $T^{(1)}$ and $T^{(2)}$, and a value for β_{rot}. The value of θ_{bond}, nominally 90°, was adjusted over a ±5° range when needed to account for proton cross-peak positions measured in HYSCORE experiments.

RESULTS

The inset to Figure 1 shows the cw-EPR spectrum of **1·NO** collected at 9.68 GHz. The spectrum shows an axial line shape with features at g = 4 and 2. Figure 1a shows an expanded plot of the g = 4 feature, with the experimental data being given in black and a best-fit simulation in red. The simulation was done with $|E|/D$ = 0.001, ΔH_x = 200 MHz, and ΔH_y = 360 MHz and yielded χ_n^2 = 0.2. Because strain in the ZFS parameters D and E was not included in our calculations, the line-width parameters ΔH_x and ΔH_y consist of contributions from strain in the ZFS parameters, and the typical magnetic and dynamic interactions that contribute to the intrinsic line shape. This simplified approach to analysis of the cw-EPR data was chosen because only the $|E|/D$ and g_0 values are needed for ESEEM and HYSCORE simulations. Parts b and c of Figure 1 show the g = 4 region of the cw-EPR spectra (black traces) collected for **2·NO** and **3·NO**, respectively. The simulations of this spectral feature (red traces) yielded best-fit values for $|E|/D$, ΔH_x, and

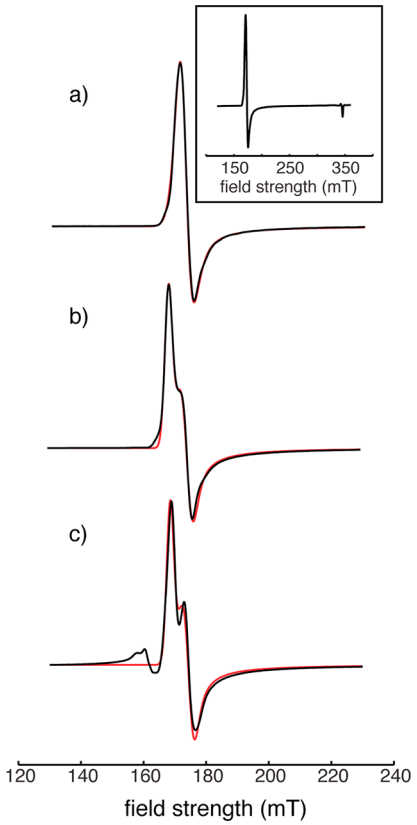

Figure 1. cw-EPR spectra (black traces) showing the g = 4 feature of (a) **1·NO**, (b) **2·NO**, and (c) **3·NO** in aqueous buffer. The inset shows the full EPR spectrum for **1·NO**. The microwave frequencies used for data acquisition were (a) 9.6773, (b) 9.6802, and (c) 9.6691 GHz. The other parameters for data acquisition are given in the Experimental Section. The red traces are simulations using $S = {}^3/_2$, D = 3.0e + 5 MHz, and g_0 = 2.015 as common parameters. (a) $|E|$ = 340 MHz, $\Delta H_{x,y}$ = (200, 360) MHz. (b) $|E|$ = 3430 MHz, $\Delta H_{x,y}$ = (210, 160) MHz. (c) $|E|$ = 3450 MHz, $\Delta H_{x,y}$ = (200, 150) MHz.

ΔH_y that were nearly identical, with $|E|/D$ = 0.01 being found for both complexes. While χ_n^2 was still well below 1 (0.5) for **2·NO**, the value for **3·NO** was 1.6. Figure 1c shows that this higher χ_n^2 value stems from an additional EPR signal at g = 4.3 that is most likely due to Fe^{III} contamination. This finding is consistent with a previous study of ferrous complexes of **1**−**3** that showed that the $Fe^{II}N_2O_3$ complex was readily oxidized when exposed to air.[32]

Figure 2a shows a three-pulse ESEEM spectrum collected at 280 mT (g = 2.47; see the inset) for **2·NO**. The spectrum shows several broad features that arise primarily from the hyperfine couplings of the coordinated nitrogen atoms of NO and the N_2O_2 ligand, the protons of bound water, and the protons of the N_2O_2 ligand. At 280 mT, the ^{14}N and ^1H Larmor frequencies are 0.9 and 11.9 MHz, respectively, which lead to a substantial overlap of their contributions to the ESEEM spectrum. The resulting spectral congestion was nicely sorted into different quadrants of the four-pulse HYSCORE spectrum, as shown in the contour plot of Figure 2b. Because the hyperfine couplings of the coordinated ^{14}N atoms are much greater than the ^{14}N Larmor frequency, most of their cross-peak intensity is resolved in the (−, +) quadrant.[28] Therefore, the minor cross peaks at (−3.4, 11.8), (−4.3, 9.6), and (−5.2, 7.8) and the more intense cross peak at (−4.7, 5.7) MHz, along with their complementary correlation peaks on the opposite

DOI: 10.1021/acs.inorgchem.5b00788
Inorg. Chem. 2015, 54, 6486−6497

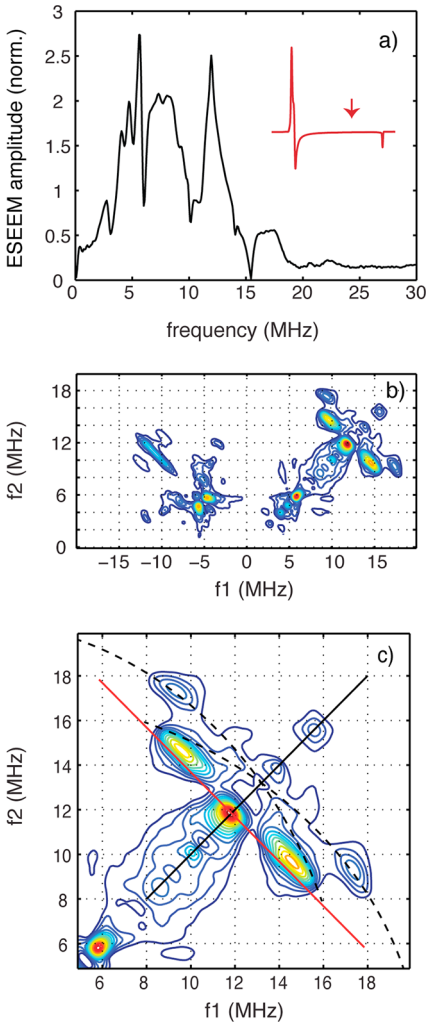

Figure 2. (a) Three-pulse ESEEM and (b and c) four-pulse HYSCORE spectra of **2·NO** in aqueous buffer. Data were collected at 280 mT (inset in part a) using a τ value of 84 ns. The other measurement parameters were provided in the Experimental Section. The frequency diagonal (black line), antidiagonal (red line), and coupling ridges (dashed curves) were placed on part c using drawing software.

side of this quadrant's frequency diagonal, can be assigned to ^{14}N. For both quadrants of the HYSCORE spectrum, cross peaks will be referred to by their location above or to the more positive f2 side of the frequency diagonal.

For protons, hyperfine couplings are most often less than the Larmor frequency and as such their cross peaks are resolved in the (+, +) quadrant. Figure 2c shows an expansion of the HYSCORE spectrum of Figure 2b about the ^{1}H Larmor frequency of 11.9 MHz. The off-diagonal cross peaks that arise from coupled protons are located at (9.4, 17.3) and (9.6, 14.6) MHz. The red line drawn on Figure 2c was constructed perpendicular to the frequency diagonal (black line), so that it intersects the frequency diagonal at the ^{1}H Larmor frequency of 11.9 MHz. This red line is referred to as the "^{1}H antidiagonal" and can be used as a reference point for measuring the dipolar, or anisotropic, portion of the hyperfine coupling. Specifically, for powder samples, hyperfine couplings with large dipolar contributions are predicted to yield "ridges" or "arc-shaped" HYSCORE cross peaks that will be shifted to the high-frequency side of the antidiagonal in proportion to $T^2/|\omega_p|$, where T is the dipolar coupling (eq 4) and ω_p is the proton Larmor frequency.[27,41,42] Because the dipolar couplings of bound water protons are expected to be large, the cross peak at (9.4, 17.3) MHz is the best candidate for assignment to bound water because it shows the largest displacement from the ^{1}H antidiagonal (Figure 2c).

The cross-peak contour centered at (9.4, 17.3) MHz at 280 mT shows only a modest curvature because of the limited set of molecular orientations sampled at this field position.[43] To characterize the hyperfine coupling and extract structural information regarding the ligand orientation with respect to the Fe−NO bond, the HYSCORE experiment was repeated at several magnetic field positions across the EPR spectrum. In principle, one expects the cross peaks for these protons to follow ridge trajectories, like those sketched in Figure 2c (dashed curves), as one changes the observation field. Figure 3 shows a series of five HYSCORE spectra collected across the EPR spectrum for **2·NO**. The cross peak centered at (9.4, 17.3) MHz at 280 mT tracks to (7.6, 17.6) MHz at 260 mT and then to (6.0, 17.6) MHz as one lowers the magnetic field to 240 mT. This cross peak is not resolved as one approaches the extremes of the EPR spectrum at 200 and 320 mT. The other proton correlation, centered at (9.6, 14.6) MHz at 280 mT is of higher intensity and tracks with the ^{1}H antidiagonal (red lines in Figure 3) with magnetic field. This cross peak represents a composite of contributions from the 14 ^{1}H atoms of the N_2O_2 ligand, as confirmed below. The proximity of this cross peak to the ^{1}H antidiagonal and the modest changes that occur in its shape as the field is varied from 200 to 320 mT show that these ^{1}H atoms are characterized by weaker hyperfine couplings, clearly distinguishing their spectral contribution from those attributed to bound water.

Figure 4 shows HYSCORE contour plots for **1·NO** at field positions that range from 220 to 300 mT across the EPR spectrum. Cross peaks that originate from fundamental ^{1}H hyperfine frequencies, $(\omega_\alpha, \omega_\beta)$, and that follow a ridge trajectory, similar to those assigned to the ^{1}H atoms of the water ligand of the N_2O_2 complex, are resolved over a magnetic field range from 240 to 300 mT. These correlations are centered at the following frequency and field positions: (5.9, 17.6) MHz, 240 mT; (7.3, 17.6) MHz, 260 mT; (9.3, 17.3) MHz, 280 mT; (10.5, 17.4) MHz at 300 mT. They differ from those of **2·NO** in that they are more intense because of contributions from a second water ligand and they have a different contour shape, reflecting differences in the coordination for the two bound water molecules. The HYSCORE spectrum collected at 220 mT shows a diffuse cross peak at (11.7, 17.6) MHz that is a "combination-frequency" peak of the form $(|\omega_\alpha - \omega_\beta|, \omega_\beta)$ arising from the presence of more than one strongly coupled water proton.[41] The strong cross peak resolved along the frequency diagonal just below 18 MHz at 220 and 240 mT is a sum combination frequency peak, $(\omega_\alpha + \omega_\beta, \omega_\beta + \omega_\alpha)$, that consists of contributions from both four-pulse HYSCORE and three-pulse ESEEM.

Figure 5 shows HYSCORE contour plots collected for the **3·NO** sample at the three field positions 240, 260, and 280 mT, where the strongest cross peaks attributed to water were resolved for **2·NO** and **1·NO**. The cross peaks attributed to bound water molecules for **2·NO** (Figure 3) and **1·NO** (Figure 4) are absent from these data, while those that lie near the ^{1}H antidiagonal remain. This observation is consistent with the lack of labile sites available for water binding in **3·NO** because of coordination of the pentadentate ligand and NO. These

DOI: 10.1021/acs.inorgchem.5b00788
Inorg. Chem. 2015, 54, 6486−6497

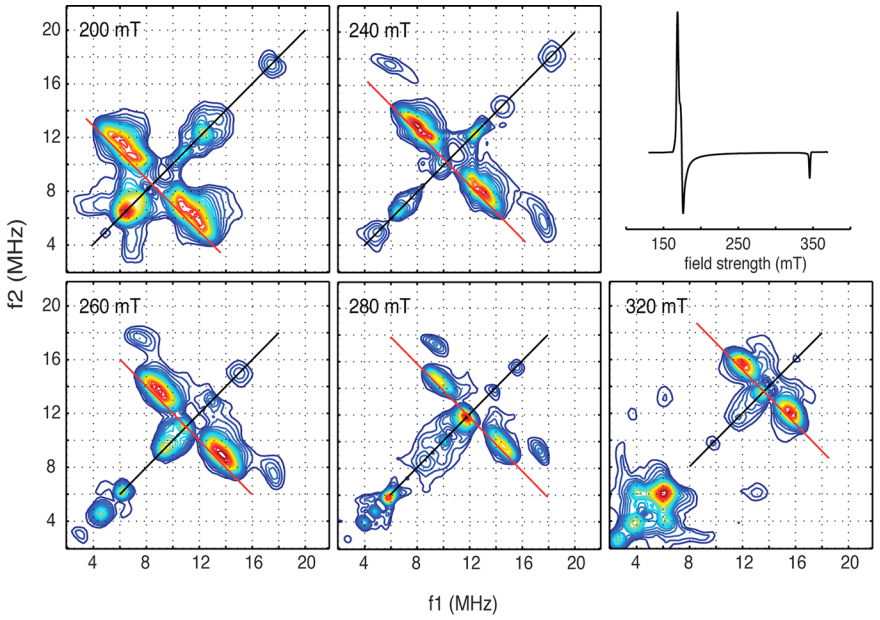

Figure 3. HYSCORE spectra collected for **2·NO** as a function of the magnetic field strength. The τ values used for data acquisition were as follows: 116 ns, 200 mT; 96 ns, 240 mT; 92 ns, 260 mT; 84 ns, 280 mT; 148 ns, 320 mT. The cw-EPR spectrum is provided in the upper right panel. Cross-peak intensities are color-coded, ranging from blue (weakest) to dark red (strongest).

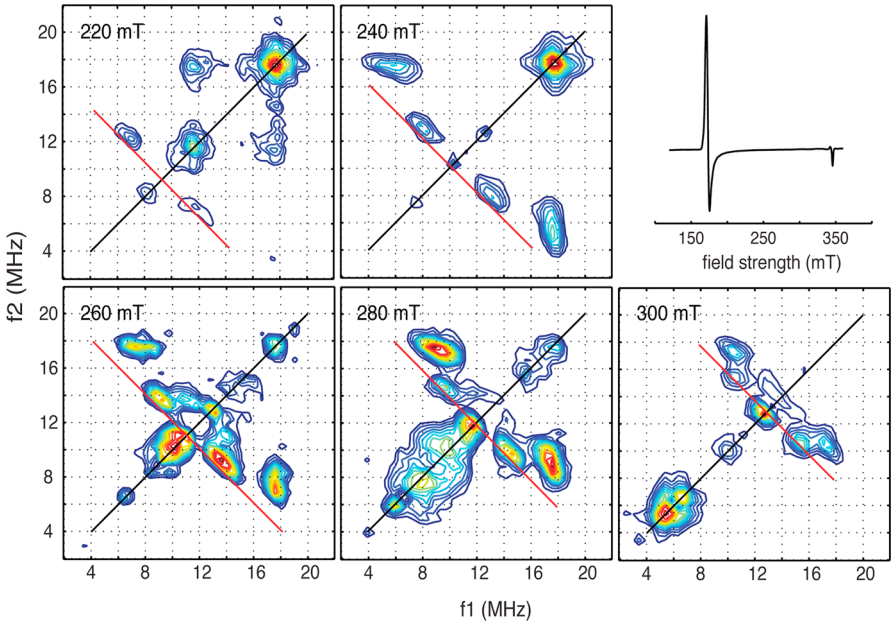

Figure 4. HYSCORE spectra collected for **1·NO** as a function of the magnetic field strength. The τ values used for data acquisition were as follows: 108 ns, 220 mT; 96 ns, 240 mT; 92 ns, 260 mT; 84 ns, 280 mT; 80 ns, 300 mT.

results confirm the assignments of the ^{1}H cross peaks made above. A more conventional way to confirm these assignments is to collect a parallel set of ESEEM or HYSCORE data in $^{2}H_2O$ buffer and show that the peaks are exchangeable. Unfortunately, for these model complexes, strong ^{2}H ESEEM led to extensive cross-suppression and the loss of peaks due to ^{14}N and nonexchangeable protons.[44] An example of these cross-suppression effects is provided as Supporting Information (SI; Figure S1).

^{1}H HYSCORE data were analyzed by computer simulation to determine hyperfine coupling parameters and the orientation of the coupled water protons with respect to the PAS of the ZFS. Because **2** features two symmetrical labile sites, its NO adduct, **2·NO**, has just one chemically distinct labile position for the binding of a water molecule. Our analysis focused on the cross peaks that were resolved at (6.0, 17.6), (7.6, 17.6) and (9.4, 17.3) MHz at field positions of 240, 260, and 280 mT, respectively (Figure 3). All three of these cross peaks show simple contours with a single amplitude maximum and appear to have a ridge- or arc-shaped contour. This shape is most prominent for the spectrum collected at 240 mT. Considering that the z axis of the ZFS tensor is along the Fe−NO bond[24] and taking (θ_{bond}, ϕ_{bond}) = (90°, 0°), the two protons of a coupled water molecule would have equivalent, absolute-value projections along the z axis for β_{rot} and $\Delta\beta$ values of 30° and 120°, respectively (Scheme 2). Starting our analysis with these

DOI: 10.1021/acs.inorgchem.5b00788
Inorg. Chem. 2015, 54, 6486−6497

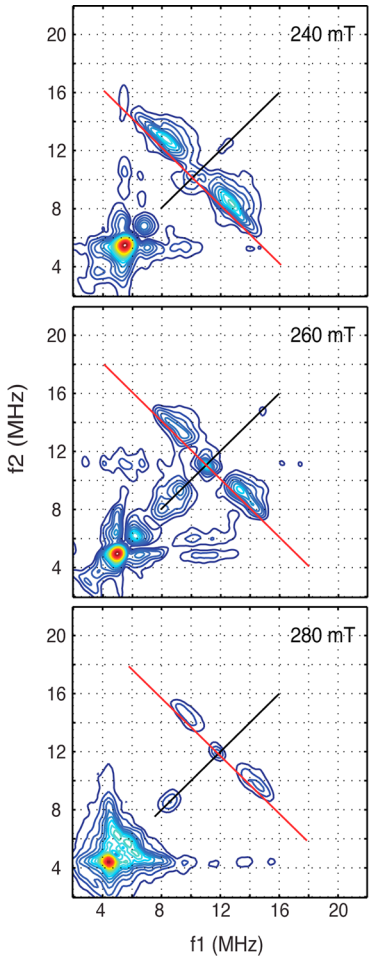

Figure 5. Four-pulse HYSCORE spectra collected for **3·NO** in aqueous buffer over the field range where cross peaks assigned to coordinated water molecules are well resolved. τ values for the field positions shown were as follows: 96 ns, 240 mT; 92 ns, 260 mT; 84 ns, 280 mT.

values for orienting the proton hyperfine coupling tensors (eqs 5−8) and selecting a value for the dipolar coupling, T, of 5 MHz using the simple geometric picture of Scheme 2a, we obtained reasonable simulations of our HYSCORE data. To match the frequency position and cover the extent of the maxima for each cross peak, it was necessary to reduce the dipolar coupling for both water protons to T = 4.8 MHz and the value used for β_{rot} to 23° ($\Delta\beta$ = 120°). An identical set of simulations would be realized for β_{rot} = 37° ($\Delta\beta$ = 120°), as the absolute-value projections of the water protons along the Fe−NO bond would be unchanged. The results of these simulations are shown as black contours superimposed on the ^{1}H HYSCORE data of **2·NO** and are given in Figure 6. The simulations of the ^{1}H HYSCORE response at 240, 260, and 280 mT show that this simple water coupling model accounts well for the positions and extent of the cross peaks that are split well off the ^{1}H antidiagonal. They also predict that cross peaks arising from the fundamental ^{1}H hyperfine coupling frequencies will only be observed over the 240−280 mT field range for the magnetic field positions reported here. A second peak resolved along each coupling ridge close to the ^{1}H antidiagonal is also predicted. This simulated ^{1}H HYSCORE response is a consequence of the cis orientation of the coordinated water with respect to the Fe−NO bond and the set of molecular orientations that are in resonance at the intermediate magnetic field positions studied. Because the water protons are oriented so that the principal axis of their hyperfine coupling tensor, $A_{\|}$ or 2T, is nearly perpendicular to the Fe−NO bond, the molecular orientations sampled at 240−280 mT are weighted by both $A_{\|}$ and $A_{\perp}$. The "coupling ridges" shown as dashed lines superimposed on Figure 2c describe the location of the cross peaks for an experiment where all molecular orientations are in resonance at once, and they approach the antidiagonal at the $A_{\perp}$ and $A_{\|}$ extremes of the tensor. The simulations in Figure 6 show two cross peaks along each coupling arc, one near $A_{\perp}$ and, therefore, close to the ^{1}H antidiagonal and the second at a frequency that involves an orientation-averaged value that includes $A_{\|}$ and is resolved in a clean spectral window well

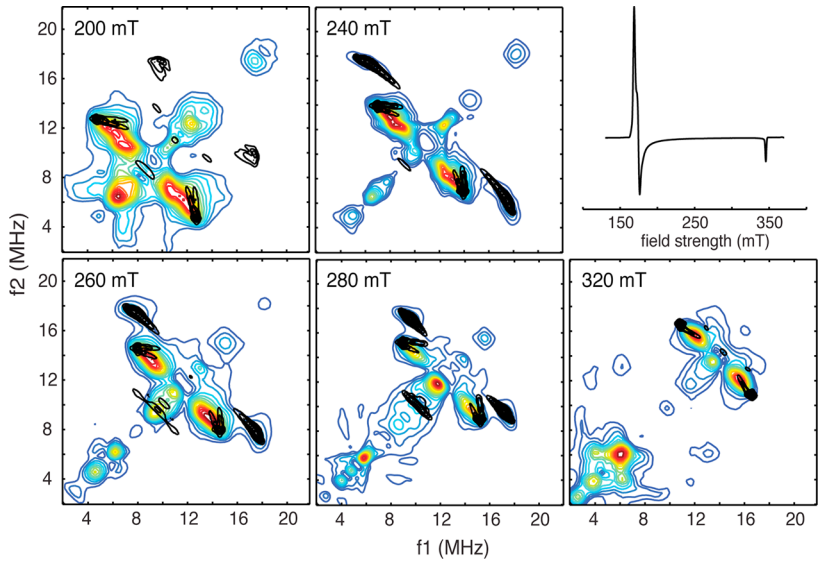

Figure 6. Comparison of the ^{1}H HYSCORE spectra of **2·NO** with simulations (black contours) done considering a single bound water molecule described by (θ_{bond}, ϕ_{bond}) = (90°, 0°), $T^{(1)} = T^{(2)}$ = 4.8 MHz, β_{rot} = 23°, $\Delta\beta$ = 120°, D = 3.0e + 5 MHz, E = 3440 MHz, microwave frequency = 9.68 GHz, $S = {}^3/_2$, and g_0 = 2.015. τ values matched those used in the experiments (Figure 3 caption).

DOI: 10.1021/acs.inorgchem.5b00788
Inorg. Chem. 2015, 54, 6486−6497

separated from the antidiagonal. A final comment about the simulations shown in Figure 6 is that they also predict the presence of weak cross peaks at (9.9, 17.3) MHz at 200 mT that were not observed in our experiments. These predicted cross peaks arise from correlations between combinations of ^{1}H hyperfine frequencies and are a consequence of the presence of two strongly coupled protons. It is likely that these cross peaks were below the noise floor of our measurement at 200 mT for **2·NO**. However, pH titrations of $Fe^{II}(N_2O_2)$ predict that at pH 6.5 the two labile coordination sites will be occupied by a 4:1 molar mixture of H_2O and OH^-. Such a mixture would mean that 20% of the **2·NO** complexes contributing to the HYSCORE have only one coupled proton and would not contribute to the predicted combination cross peak.

The ^{1}H HYSCORE response from the bound water protons of **1·NO** differs from that of **2·NO** in terms of cross-peak contour shape and intensity. Figure 7 shows expanded views of the cross peaks assigned to water protons at 240 mT that are resolved at (6.0, 17.6) MHz for **2·NO** (Figure 7a) and (5.9, 17.6) MHz for **1·NO** (Figure 7b,c). The data are represented with filled contours that are coded blue for weak intensity and dark red for highest intensity. The cross peak resolved for **2·NO** (Figure 7a) is weaker and has a shape that reveals the ridge trajectory expected for a coupled proton. The black contour superimposed on this cross peak is a simulation that uses the coupling parameters given above and shows that the simple model used there does a good job of accounting for the cross-peak position and contour shape. For **1·NO** (Figure 7b,c), the contour shape is substantially different in that its trajectory appears to be almost parallel to the f1 frequency axis rather than curving inward toward the frequency diagonal. This difference in contour shape is accentuated in Figure 7b, where the **1·NO** ^{1}H HYSCORE data collected at 240 mT (filled contours) are compared with the single water simulation (black contours) that adequately described the **2·NO** data set of Figure 7a. Clearly, the hyperfine couplings of the two water molecules coordinated to iron for **1·NO** must differ in a fashion that will account for the contour shape. Because the cross peaks arising from individual water protons are not resolved in our experiments, these data most likely represent an ensemble of water conformers that were frozen in when the sample was prepared. In an attempt to account for the >4 MHz spread in the contour along the f1 axis with a corresponding spread in frequency correlations of about 1 MHz along the f2 axis, we explored the effects of distributions in rotation about the Fe–OH_2 bond, β_{rot}, the dipolar coupling, T, and the polar angle describing the orientation of the Fe–OH_2 bond, θ_{bond}. We found that the most straightforward way to account for dispersion of the ^{1}H contours parallel to the frequency axes was to allow for small deviations of θ_{bond} from 90°. The simulation shown as the black contour of Figure 7c considers two coupled water molecules with discrete orientations. The first water was characterized by $(\theta_{bond}, \phi_{bond}) = (86.5°, 0°)$, $\beta_{rot} = 26°$, $T^{(1)} = 4.6$ MHz, and $T^{(2)} = 4.9$ MHz, where each water proton was assigned a different dipolar coupling. The second water was characterized by parameters similar to those used for the water proton couplings of **2·NO**: $(\theta_{bond}, \phi_{bond}) = (90°, 90°)$, $\beta_{rot} = 23°$, $T^{(3)} = 4.7$, and $T^{(4)} = 4.8$ MHz. This model yields cross peaks of comparable intensity that combine to account for the contour shape arising from the coupled water ^{1}H atoms of **1·NO**. Figure 8 provides a comparison of the full ^{1}H HYSCORE data set obtained for **1·NO** (color contours) with simulations (black contours) done using this two-water model. The frequency positions and contour shapes are well-predicted at all five field positions from 220 to 300 mT. The simulations also show that correlations from the water ^{1}H hyperfine frequencies are only observed over the range of magnetic fields from 240 to 300 mT and that the HYSCORE signature of bound water at 220 mT is given by weak cross peaks centered at (11.7, 17.6) MHz that arise from the correlation of a difference hyperfine combination frequency, $|\omega_\alpha - \omega_\beta|$, and a fundamental frequency, ω_β.

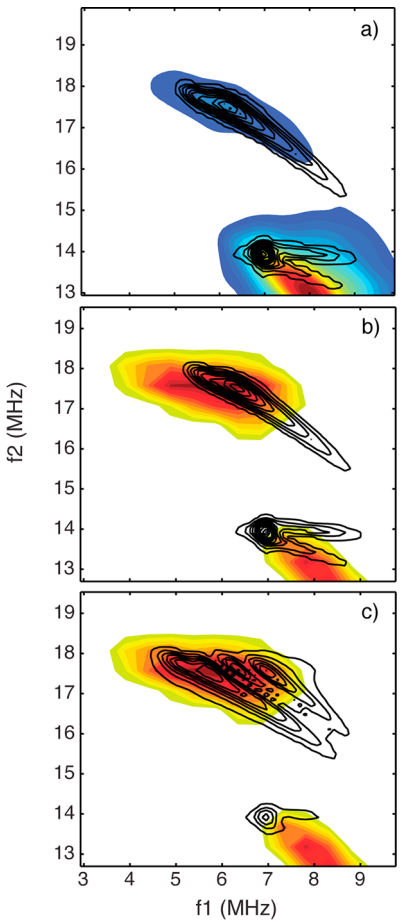

Figure 7. Comparison of water ^{1}H cross-peak shapes and frequency positions for HYSCORE data collected at 240 mT and τ = 96 ns for (a) **2·NO** and (b and c) **1·NO**. The data are shown as filled contours and are color-coded for intensities ranging from blue (weakest) to dark red (strongest). The black contours are computer simulations of the data. For parts a and b, these simulations consider a single water molecule with $(\theta_{bond}, \phi_{bond}) = (90°, 0°)$, $T^{(1)} = T^{(2)} = 4.8$ MHz, and $\beta_{rot} = 23°$. For part c, two water molecules are considered with $(\theta_{bond}, \phi_{bond}) = (86.5°, 0°)$ and (90°, 90°), $T^{(1,2)} = (4.6, 4.9)$ and $T^{(3,4)} = (4.7, 4.8)$ MHz, and $\beta_{rot}^{(1)} = 26°$ and $\beta_{rot}^{(2)} = 23°$.

DISCUSSION

This study was motivated by our desire to characterize the coordination chemistry of Fe^{II} at the catalytic site of a pterin-dependent amino acid hydroxylase, phenylalanine hydroxylase (PheH). An important question in understanding the structural changes that accompany allosteric activation of the enzyme, the binding of substrate L-phe, and/or the binding of cofactor pterin, involves quantifying water coordination to the metal ion. The nitrosyl adducts of **1**–**3** that were chosen for this study showed cw-EPR spectra typical for high-spin $S = {}^3/_2$ systems

DOI: 10.1021/acs.inorgchem.5b00788
Inorg. Chem. 2015, 54, 6486–6497

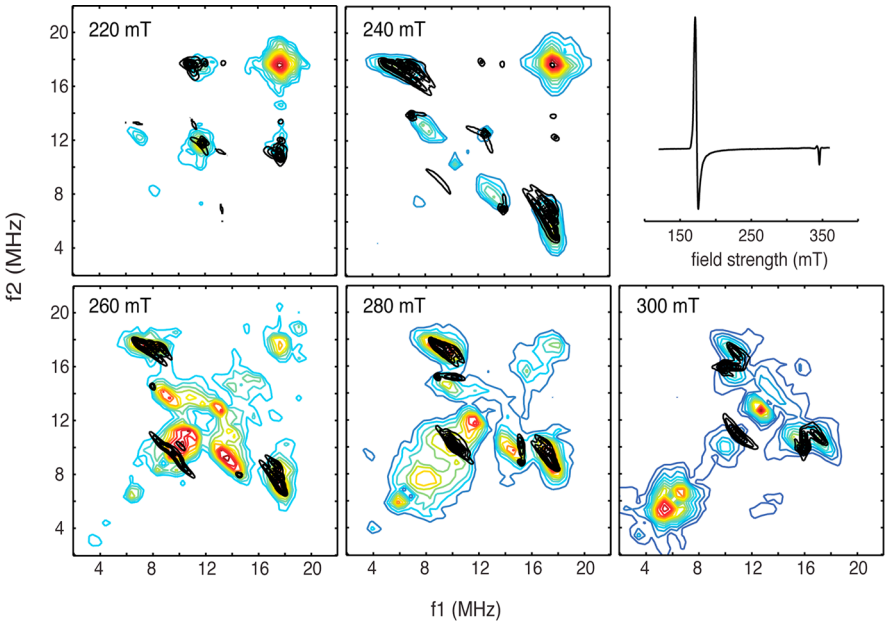

Figure 8. Comparison of the ^{1}H HYSCORE spectra of **1·NO** with simulations (black contours) done considering two bound water molecules described by (θ_{bond}, ϕ_{bond}) = (86.5°, 0°), $T^{(1,2)}$ = (4.6, 4.9) MHz, and β_{rot} = 26° and (θ_{bond}, ϕ_{bond}) = (90°, 90°), $T^{(3,4)}$ = (4.7, 4.8) MHz, and β_{rot} = 23°. $\Delta\beta$ = 120° for both water molecules. Other EPR parameters needed for these simulations were as follows: microwave frequency, 9.68 GHz; *S*, $^{3}/_{2}$; *D*, 3.0e + 5 MHz; *E*, 340 MHz; g_0, 2.015. τ values matched those used in the experiments (Figure 4 caption).

with near-axial symmetry, similar to those measured for {FeNO}^{7} adducts of PheH, tyrosine hydroxylase (TyrH) and taurine dioxygenase (TauD). Furthermore, these model complexes yielded ESEEM and HYSCORE spectra characterized by ^{14}N and ^{1}H modulations of intensity and frequency similar to those observed in previous studies of {FeNO}^{7} derivatives of the nonheme iron hydroxylases mentioned above.[31,45,46] These findings, coupled with the facial coordination of the base N_2O ligand to Fe^{II}, make the model complexes studied in this work excellent magnetic models for interpreting HYSCORE and ESEEM spectra obtained from NO adducts of the enzymes.

The ^{1}H HYSCORE spectra of **1·NO** (Figure 4) and **2·NO** (Figure 3) show that cross peaks arising from coordinated water ligands are resolved in a clean spectral window over a field range from 240 mT (g = 2.9) to 300 mT (g = 2.3). At the low-field (g = 4.0) and high-field (g = 2.0) ends of the spectrum, the cross peaks predicted by our simulations are found near the $\omega_p \pm |T|$, or $\omega_p \pm |A_\perp|$, position along the ^{1}H antidiagonal, where they overlap with contributions from the more weakly coupled protons of the N_2O_x ligands. Both of these observations are a consequence of orientation selection.[43,47] Because the water ligands are bound cis to the Fe–NO bond, as the resonance field position approaches g = 2, their HYSCORE cross-peak positions are determined by $A_\perp = -T$. At the opposite end of the EPR spectrum, near g = 4, the cross-peak contours take on the full dispersion of hyperfine frequency combinations ranging from $-T$ to $+2T$, or $A_\perp$ to $A_\parallel$, and when combined with the increase in the effective value of T that occurs as one goes to lower field, only the contributions near the ^{1}H antidiagonal are predicted.[20,48] Unfortunately, for our initial studies of PheH, ESEEM and HYSCORE data were only collected in the g = 4 and 2 regions of the EPR spectrum, where the contributions from bound water ligands overlap contributions from the weakly coupled protons of the coordinated histidylimidazole side chains, the side chain of the glutamic acid ligand, and the surrounding protein matrix. With this knowledge in hand, subsequent HYSCORE studies of {FeNO}^{7} adducts of PheH, TyrH, and TauD have shown ^{1}H cross peaks that can be assigned to bound H_2O or OH^- ligands. The model compound work presented here was instrumental in defining the spectral window in which these ligand hyperfine couplings could be resolved.

Our analysis of the HYSCORE response measured for the water ligand of **2·NO** shows that the simple model depicted in Scheme 2 and used for determining Euler angles and estimating the strength of the dipolar coupling is reasonable. A consequence of the narrow range of magnetic field strengths, 240–300 mT, for which cross peaks from the coupled protons can be observed is that our analysis of the hyperfine couplings is based on a limited set of molecular orientations. This makes it difficult to distinguish isotropic, A_{iso}, and anisotropic, T, contributions to the hyperfine coupling using the cross-peak position as the sole criterion for analysis. Simulations of the **2·NO** ^{1}H HYSCORE data showed that the correlation frequencies at 240, 260, and 280 mT could be predicted within a ±0.2 MHz window using A_{iso} values that varied from 0.0 to 1.3 MHz, with concomitant adjustment of T from 4.8 to 4.1 MHz. While this range of A_{iso} values could be compensated for by the dipolar coupling to provide a reasonable simulation of cross-peak positions, the values of A_{iso} and T also determine the curvature of the coupling ridge that gives rise to the contour shape of the cross peaks.[27,41,49] In our simulations, the interplay between A_{iso} and T in determining the contour shape was most evident at 240 mT, where the largest set of molecular orientations are selected. The simulations that best accounted for the cross-peak position and contour shape were those with A_{iso} = 0.0 ± 0.3 MHz and T = 4.8 ± 0.2 MHz (Table 1). Simulations superimposed on the contour shapes for the HYSCORE spectra of **2·NO** that support these findings are shown in Figure S2 in the SI.

DOI: 10.1021/acs.inorgchem.5b00788
Inorg. Chem. 2015, 54, 6486–6497

Table 1. Spin Hamiltonian Parameters from EPR and HYSCORE Spectral Analysis

complex	$\lvert E\rvert/D$	$\Delta H_{x,y}$ (MHz)	ligand	T (MHz)	β_{rot} (deg)	$\Delta\beta$ (deg)
3·NO $\{FeNO\}^7(N_2O_3)$	0.011	200, 150				
2·NO $\{FeNO\}^7(N_2O_2)(H_2O)$	0.011	210, 160	water 1	4.8, 4.8	23	120
1·NO	0.001	200, 360	water 1	4.6, 4.9	26	120
			water 2	4.7, 4.8	23	120

HYSCORE spectra collected for **1**·NO show an increase in the water ^{1}H cross-peak intensity and a change in the contour shape compared to data from **2**·NO. Our analysis of these changes involved adding a second water molecule and adjusting its bond angle, θ_{bond}, and the dipolar coupling for the ligand's protons to values that would account for the contour shape of the cross peaks assigned to bound water from 240 to 300 mT. This was accomplished by holding A_{iso} at 0.0 MHz and adjusting T so that it varied over the group of four coupled protons from 4.6 to 4.9 MHz. This variation in the dipolar coupling is modest because eq 4 can be used to show that it represents a difference in the dipolar distances of just 0.05 Å. While our model accounts for the contour shapes, it also yields simulations that show discrete cross peaks for each coupled proton, a feature that was not observed for either **1**·NO or **2**·NO. This lack of resolution likely stems from rotameric distributions of water molecules that are frozen in when the samples are prepared, distributions in the dipolar coupling that are magnified by the proximity of the ligand protons to the paramagnetic center, and variations in the ligand coordination with respect to the Fe(N_2O_x) framework. This last point is problematic for **1** because it has three open-coordination sites. Full HYSCORE spectra collected at 280 mT are shown for all three complexes in Figure S3 in the SI. For **3**·NO and **2**·NO, well-resolved ^{14}N cross peaks are present in the (−, +) quadrant. Using the Fe−NO bond as our reference, both of these complexes are characterized by an equatorial coordination of 1N3O, with the remaining ligand ^{14}N being trans to the Fe−NO bond. In contrast, the HYSCORE spectrum of **1**·NO shows only a weak ^{14}N response at 280 mT (Figure S3 in the SI, top) making it difficult to determine the cross-peak positions in the (−,+) quadrant. For this complex, NO can bind so that it is cis to both ^{14}N atoms of the ligand or in two configurations, where one ^{14}N atom is cis and the other trans. Because the ^{14}N nuclei of the N_2O ligand are chemically different, all three of these complexes will yield a different HYSCORE response. The resulting spectral dispersion provides a reasonable explanation for the poor quality of the ^{14}N HYSCORE spectra observed for **1**·NO. It follows that this combination of structures also contributes to both dispersion in the coupling parameters evident in the ^{1}H HYSCORE response from bound water and the increased intrinsic line-width parameter ΔH_y determined from analysis of the cw-EPR spectrum (Figure 1 and Table 1).

One of the goals of this study was to use **1**·NO and **2**·NO to work out a method for quantifying the number of water molecules coordinated to $\{FeNO\}^7$ adducts of nonheme iron hydroxylases. Previous HYSCORE studies of aquo met-myoglobin showed that the water molecule bound axially to the $S = {}^5/_2$ ferric heme center gave rise to two discrete coupling ridges, reflecting a difference in hydrogen bonding between the water protons and distal histidine.[29] Preliminary work on PheH and TauD has shown that discrete conformations of bound water ligands are coordinated to some of the $\{FeNO\}^7$ adducts because cross peaks are resolved for each coupled proton. For these cases, one can distinguish the number of bound water molecules by tracking the cross-peak movement as a function of the field and counting the number of distinct cross peaks and coupling ridges. The resolution of individual ridges also allows for a more accurate assessment of A_{iso} and T that may provide important information needed to distinguish H_2O from OH^- coordination.

HYSCORE studies of TyrH have shown cross-peak resolution that is intermediate between the cases represented by PheH and TauD and the model complexes studied here. In this case, the contour shapes of the cross peaks carried information on the minimum number of coupled protons that need be considered in the analysis, but an additional means for quantification was needed.[50] Even for cases where cross-peak resolution is sufficient to "count" protons, complications can occur from the presence of mixtures of $\{FeNO\}^7$ species.[46] In both of these cases, an additional measure of the number of coupled water protons can be gained from analysis of their three-pulse ESEEM spectral amplitudes.[15] The **2**·NO and **1**·NO model complexes showed three-pulse ESEEM spectra that were complicated by the overlap of modulations from ^{14}N and ^{1}H couplings. The HYSCORE spectra for these two complexes (Figures 3 and 4) indicate that the cleanest window for performing an ESEEM amplitude analysis is over the high-frequency portion of the ^{1}H ESEEM response assigned to bound water that ranges from 15 to 20 MHz. Unfortunately, the three-pulse ESEEM data collected for these samples also show a substantial ^{1}H combination peak at 17.6 MHz that complicates the analysis. Figure S4 in the SI shows a comparison of the three-pulse ESEEM spectra collected for **2**·NO and **1**·NO at 240, 260, and 280 mT. The amplitude of the ^{1}H combination peak is most intense at 240 mT and falls off in intensity as one moves to higher field. This trend can also be observed in the HYSCORE spectra from these complexes because the peaks along the frequency diagonal are dominated by three-pulse ESEEM contributions that contaminate the spectra. The data collected for **1**·NO (Figure 4) at 240 mT show its water proton HYSCORE cross peak at (5.9, 17.6) MHz, together with an intense combination peak along the frequency diagonal at 17.6 MHz. At 280 mT, the situation is reversed in that the water proton cross peak centered at (9.3, 17.3) MHz is much more intense than the combination peak along the frequency diagonal at 17.6 MHz. Therefore, the spectral window for using three-pulse ESEEM spectra to determine the number of bound water molecules was chosen to be from 15.8 to 20.0 MHz at 280 mT. Three-pulse ESEEM spectra collected at 280 mT are shown for **1**·NO and **2**·NO in Figure 9a. The time-domain ESEEM data used to obtain these spectra were normalized by the division of a biexponential background decay function prior to processing for the purpose of comparing the integrated intensities from 15.8 to 20.0 MHz. For **2**·NO, we measured an integrated intensity of 20.4, while for **1**·NO, an intensity of 31.4 was found. To test how reliable this approach might be for quantifying bound water, we also performed three-pulse ESEEM simulations at 280 mT using the water proton couplings and tensor orientations that were determined by HYSCORE analysis (Figure 9b). For the simulations, the time domain output of *EasySpin* was

DOI: 10.1021/acs.inorgchem.5b00788
Inorg. Chem. 2015, 54, 6486−6497

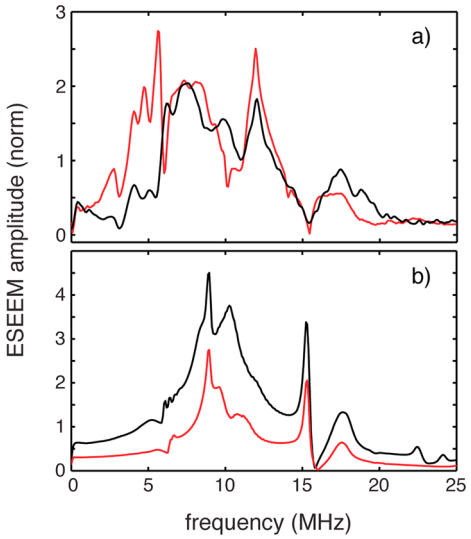

Figure 9. (a) Three-pulse ESEEM data collected at 280 mT (τ = 84 ns) for the **1·NO** complex (black) versus the **2·NO** complex (red). (b) Three-pulse ESEEM simulations done using the following spin Hamiltonian parameters. For the **2·NO** complex (red): A_{iso}, 0.0 MHz; $T^{(1,2)}$ = (4.8,4.8) MHz; β_{rot}, 30°; $\Delta\beta$, 120°; (θ_{bond}, ϕ_{bond}), (90°, 0°), E, 3440 MHz. For the **1·NO** complex (black): A_{iso}, 0.0 MHz; $T^{(1,2)}$, (4.6, 4.9) MHz; β_{rot}, 26°; (θ_{bond}, ϕ_{bond}), (86.5°; 0°), and for the second water, $T^{(3,4)}$, (4.7, 4.8) MHz; β_{rot}, 23°; (θ_{bond}, ϕ_{bond}), (90°, 90°); E, 340 MHz. Parameters common to both simulations were as follows: microwave frequency, 9.68 GHz; S, $^3/_2$; D, 3.00e + 5 MHz; τ, 84 ns.

normalized and processed in the same fashion as the experimental data. The simulated ESEEM spectra gave an integrated intensity over the range from 15.8 to 20.0 MHz for **2·NO**, or one water, of 16.2 MHz, while the two-water simulation of the three-pulse ESEEM data obtained for **1·NO** yielded an intensity of 24.7. For both experiment and simulation, intensity increases of a factor of 1.5 were realized upon the addition of a second bound water molecule. This empirical approach to quantification should be used with caution. A comparison of parts a and b of Figure 9 shows the dramatic effect that the contributions from ^{14}N and ^{1}H hyperfine couplings of the N_2O_x ligands have on the ESEEM spectra. These effects illustrate the importance of model complexes studied here because they provide a reasonable mimic of the ^{14}N and ^{1}H modulations arising from the ligands of the facial triad. However, the distributions of water orientations that are present for both **1·NO** and **2·NO** can markedly affect the ESEEM intensities.[51] Therefore, it is not clear how applicable this approach will be to studies of the mononuclear nonheme iron sites of enzymes.

SUMMARY

The model complex studies presented in this work provide a straightforward protocol for detecting and analyzing water coordination to S = $^3/_2$, {FeNO}^{7} adducts of MNOs. The simple model of bound water that was employed to guide data analysis allowed for the efficient evaluation of coupling constants and structural information while properly considering both ligand protons, and even a second coordinated water, in simulations. The importance of considering contour shapes in analysis of the HYSCORE data was also demonstrated.

ASSOCIATED CONTENT

Supporting Information

Additional HYSCORE simulations, full HYSCORE spectra, three-pulse ESEEM spectra, and three-pulse ESEEM simulations supporting arguments made in the Discussion. The Supporting Information is available free of charge on the ACS Publications website at DOI: 10.1021/acs.inorgchem.5b00788.

AUTHOR INFORMATION

Corresponding Authors

*E-mail: mccracke@msu.edu. Telephone: (517) 355-9715 (ext. 269).

*E-mail: caradonn@bu.edu. Telephone: (617) 353-1692.

Notes

The authors declare no competing financial interest.

ACKNOWLEDGMENTS

Ian Heslop and Benjamin Thompson provided help in acquiring some of the EPR data. This work was supported by funds from NSF Grant SusChEM 1300122 (to J.P.C.) and NIH Grant RR-15880 and the Michigan Economic Development Corp. (to J.M.).

REFERENCES

(1) Hegg, E. L.; Que, L. *Eur. J. Biochem.* **1997**, *250*, 625−629.
(2) Bruijnincx, P. C. A.; van Koten, G.; Gebbink, R. J. M. *Chem. Soc. Rev.* **2008**, *37*, 2716−2744.
(3) Costas, M.; Mehn, M. P.; Jensen, M. P.; Que, L. *Chem. Rev.* **2004**, *104*, 939−986.
(4) Kappock, T. J.; Caradonna, J. P. *Chem. Rev.* **1996**, *96*, 2659−2756.
(5) Fitzpatrick, P. F. *Biochemistry* **2003**, *42*, 14083−14091.
(6) Eisensmith, R. C.; Woo, S. L. C. *Adv. Genet.* **1995**, *32*, 199−271.
(7) Andersen, O. A.; Flatmark, T.; Hough, E. *J. Mol. Biol.* **2001**, *314*, 279−291.
(8) Andersen, O. A.; Flatmark, T.; Hough, E. *J. Mol. Biol.* **2002**, *320*, 1095−1108.
(9) Andersen, O. A.; Stokka, A. J.; Flatmark, T.; Hough, E. *J. Mol. Biol.* **2003**, *333*, 747−757.
(10) Shiman, R.; Jones, S. H.; Gray, D. W. *J. Biol. Chem.* **1990**, *265*, 11633−11642.
(11) Loeb, K. E.; Westre, T. E.; Kappock, T. J.; Mitic, N.; Glasfeld, E.; Caradonna, J. P.; Hedman, B.; Hodgson, K. O.; Solomon, E. I. *J. Am. Chem. Soc.* **1997**, *119*, 1901−1915.
(12) Kemsley, J. N.; Mitic, N.; Zaleski, K. L.; Caradonna, J. P.; Solomon, E. I. *J. Am. Chem. Soc.* **1999**, *121*, 1528−1536.
(13) Wasinger, E. C.; Mitic, N.; Hedman, B.; Caradonna, J. C.; Solomon, E. I.; Hodgson, K. O. *Biochemistry* **2002**, *41*, 6211−6217.
(14) Eser, B. E.; Barr, E. W.; Frantorn, P. A.; Saleh, L.; Bollinger, J. M.; Krebs, C.; Fitzpatrick, P. F. *J. Am. Chem. Soc.* **2007**, *129*, 11334−11335.
(15) Dikanov, S. A.; Tsvetkov, Y. D. *Electron Spin Echo Envelope (ESEEM) Spectroscopy*; CRC Press, Inc.: Boca Raton, FL, 1992; p 412.
(16) Rich, P. R.; Salerno, J. C.; Leigh, J. S.; Bonner, W. D. *FEBS Lett.* **1978**, *93*, 323−326.
(17) Arciero, D. M.; Lipscomb, J. D.; Huynh, B. H.; Kent, T. A.; Munck, E. *J. Biol. Chem.* **1983**, *258*, 14981−14991.
(18) Arciero, D. M.; Orville, A. M.; Lipscomb, J. D. *J. Biol. Chem.* **1985**, *260*, 14035−14044.
(19) Orville, A. M.; Chen, V. J.; Kriauciunas, A.; Harpel, M. R.; Fox, B. G.; Münck, E.; Lipscomb, J. D. *Biochemistry* **1992**, *31*, 4602−4612.
(20) Rocklin, A. M.; Tierney, D. L.; Kofman, V.; Brunhuber, N. M.; Hoffman, B. M.; Christoffersen, R. E.; Reich, N. O.; Lipscomb, J. D.; Que, L., Jr. *Proc. Natl. Acad. Sci. U.S.A.* **1999**, *96*, 7905−7909.

DOI: 10.1021/acs.inorgchem.5b00788
Inorg. Chem. 2015, 54, 6486−6497

(21) Yang, T. C.; Wolfe, M. D.; Neibergall, M. B.; Mekmouche, Y.; Lipscomb, J. D.; Hoffman, B. M. *J. Am. Chem. Soc.* **2003**, *125*, 7056−7066.
(22) Tierney, D. L.; Rocklin, A. M.; Lipscomb, J. D.; Que, L., Jr.; Hoffman, B. M. *J. Am. Chem. Soc.* **2005**, *127*, 7005−7013.
(23) Enemark, J. H.; Feltham, R. D. *Coord. Chem. Rev.* **1974**, *13*, 339−406.
(24) Aquino, F.; Rodriguez, J. H. *J. Phys. Chem. A* **2009**, *113*, 9150−9156.
(25) Brown, C. A.; Pavlosky, M. A.; Westre, T. E.; Zhang, Y.; Hedman, B.; Hodgson, K. O.; Solomon, E. I. *J. Am. Chem. Soc.* **1995**, *117*, 715−732.
(26) Atherton, N. M.; Horsewill, A. J. *Mol. Phys.* **1979**, *37*, 1349−1361.
(27) Höfer, P. *J. Magn. Reson.* **1994**, *111*, 77−86.
(28) Shane, J. J.; Höfer, P.; Reijerse, E. J.; de Boer, E. *J. Magn. Reson.* **1992**, *99*, 596−604.
(29) García-Rubio, I. s.; Fittipaldi, M.; Trandafir, F.; Van Doorslaer, S. *Inorg. Chem.* **2008**, *47*, 11294−11304.
(30) Fittipaldi, M.; Garcia-Rubio, I.; Trandafir, F.; Gromov, I.; Schweiger, A.; Bouwen, A.; Van Doorslaer, S. *J. Phys. Chem. B* **2008**, *112*, 3859−3870.
(31) Krzyaniak, M. D. *The Electron Paramagnetic Resonance Characterization of Ferrous Nitrosyl Non-Heme Iron Models and Enzymes*; Michigan State University: East Lansing, MI, 2010.
(32) Cappillino, P. J.; Miecznikowski, J. R.; Tyler, L. A.; Tarves, P. C.; McNally, J. S.; Lo, W. N.; Kasibhatla, B. S. T.; Krzyaniak, M. D.; McCracken, J.; Wang, F.; Armstrong, W. H.; Caradonna, J. P. *Dalton Trans.* **2012**, *41*, 5662−5677.
(33) Fauth, J. M.; Schweiger, A.; Braunschweiler, L.; Forrer, J.; Ernst, R. R. *J. Magn. Reson.* **1986**, *66*, 74−85.
(34) Gemperle, C.; Aebli, G.; Schweiger, A.; Ernst, R. R. *J. Magn. Reson.* **1990**, *88*, 241−256.
(35) Stoll, S.; Schweiger, A. *J. Magn. Reson.* **2006**, *178*, 42−55.
(36) Atherton, N. M. *Principles of electron spin resonance*; Ellis Horwood, PTR Prentice Hall: New York, 1993; p ix, 585 p.
(37) Brown, C. D.; Neidig, M. L.; Neibergall, M. B.; Lipscomb, J. D.; Solomon, E. I. *J. Am. Chem. Soc.* **2007**, *129*, 7427−7438.
(38) Stoll, S.; Britt, R. D. *Phys. Chem. Chem. Phys.* **2009**, *11*, 6614−6625.
(39) Roberts, J. E.; Cline, J. F.; Lum, V.; Freeman, H.; Gray, H. B.; Peisach, J.; Reinhammar, B.; Hoffman, B. M. *J. Am. Chem. Soc.* **1984**, *106*, 5324−5330.
(40) Bereman, R. D.; Kosman, D. J. *J. Am. Chem. Soc.* **1977**, *99*, 7322−7325.
(41) Schweiger, A.; Jeschke, G. *Principles of Pulse Electron Paramagnetic Resonance*; Oxford University Press: Oxford, U.K., 2001; p 578.
(42) Pöppl, A.; Kevan, L. *J. Phys. Chem.* **1996**, *100*, 3387−3394.
(43) Hurst, G. C.; Henderson, T. A.; Kreilick, R. W. *J. Am. Chem. Soc.* **1985**, *107*, 7294−7299.
(44) Stoll, S.; Calle, C.; Mitrikas, G.; Schweiger, A. *J. Magn. Reson.* **2005**, *177*, 93−101.
(45) Casey, T. M.; Grzyska, P. K.; Hausinger, R. P.; McCracken, J. *J. Phys. Chem. B* **2013**, *117*, 10384−10394.
(46) Krzyaniak, M. D.; Eser, B. E.; Ellis, H. R.; Fitzpatrick, P. F.; McCracken, J. *Biochemistry* **2013**, *52*, 8430−8441.
(47) Hoffman, B. M.; Martinsen, J.; Venters, R. A. *J. Magn. Reson.* **1984**, *59*, 110−123.
(48) Hutchison, C. A.; McKay, D. B. *J. Chem. Phys.* **1977**, *66*, 3311−3330.
(49) Dikanov, S. A.; Bowman, M. K. *J. Magn. Reson.* **1995**, *A116*, 125−128.
(50) McCracken, J.; Eser, B. E.; Mannikko, D.; Krzyaniak, M. D.; Fitzpatrick, P. F. *Biochemistry* **2015**, DOI: 10.1021/acs.biochem.5b00363.
(51) Warncke, K.; McCracken, J. *J. Chem. Phys.* **1995**, *103*, 6829−6840.

DOI: 10.1021/acs.inorgchem.5b00788
Inorg. Chem. 2015, 54, 6486−6497